ELSEVIER

Journal of Magnetism and Magnetic Materials 200 (1999) 498–514

Journal of magnetism and magnetic materials

www.elsevier.com/locate/jmmm

Spin–orbit induced magnetic phenomena in bulk metals and their surfaces and interfaces

Ruqian Wu[a,*], A.J. Freeman[b]

[a]*Department of Physics & Astronomy, California State University, Northridge, CA 91344-8268, USA*
[b]*Department of Physics & Astronomy, Northwestern University, Evanston, IL 60208-3112, USA*

Received 15 February 1999; received in revised form 16 March 1999; accepted 17 March 1999

Abstract

First-principles electronic structure studies based on local spin density functional theory and performed on extremely complex simulations of ever increasingly realistic systems, play a very important role in explaining and predicting surface and interface magnetism. This review deals with what is a major issue for first-principles theory, namely the theoretical/computational treatment of the weak spin–orbit coupling in magnetic transition metals and their alloys and its important physical consequences: magneto-crystalline anisotropy, magnetostriction, magneto-optical Kerr effects and X-ray magnetic circular dichroism. As is demonstrated, extensive first-principles calculations and model analyses now provide simple physical insights and guidelines to search for new magnetic recording and sensor materials.

Keywords: Spin–orbit coupling; Magneto-crystalline anisotropy; Magnetostriction; Magneto-optical Kerr effects; X-ray magnetic circular dichroism

1. Introduction

State-of-the-art ab initio density functional electronic structure calculations have achieved great success in the exciting field of thin film magnetism, in both explaining existing phenomena and, more importantly, in predicting the properties of new systems [1]. The prediction of enhanced magnetic moments with lowered coordination number at clean metal surfaces and interfaces has stimulated theoretical and experimental investigations for new magnetic systems and phenomena in man-made transition metal thin films, which has accompanied the renaissance of magnetism in the last decade. Many nonmagnetic materials (V, Rh, Ru and Pd) show magnetization on inert substrates [2–6]. The giant magneto-resistance in spin valves and other magnetic multilayers has already had a major impact on the magnetic recording industry [7–10].

In the relatively few years since the publication of the 100th volume of Journal of Magnetism and Magnetic Materials, significant progress has been made for the treatment of the weak spin–orbit coupling (SOC) in magnetic transition metal systems, using modern first-principles electronic structure methods, especially the highly precise full potential linearized augmented plane wave (FLAPW)

* Corresponding author. Tel.: +1-818-677-7151; fax: +1-818-677-5615.
E-mail address: ruqian.wu@csun.edu (R. Wu)

0304-8853/99/$ - see front matter
PII: S0304-8853(99)00351-0

approach [11,12]: Very reliable results for the magneto-crystalline anisotropy (MCA) energies, E_{MCA}, can now be obtained for most magnetic thin films (a few tenths meV/atom), and even for magnetic cubic bulk materials (a few μeV/atom). This enables us to solve a long-standing problem – the first-principles determination of the magnetostrictive coefficients in bulk transition metals, and their alloys and compounds with rare-earth metals. Using linear response theory, magneto-optical properties such as the magneto-optical Kerr effect (MOKE) and soft X-ray magnetic circular dichroism (MCD) can now be determined.

The aim of the present review is to provide some examples of our recent theoretical/computational developments and their applications in this exciting area using the expanded capabilities and new functionalities of the FLAPW method – including highly precise atomic forces and generalized gradient approximation (GGA) corrections to the local density approximation (LDA). The results presented here indicate that high-quality ab initio calculations of magnetic systems can achieve high accuracy and precision even for a wide range of SOC-induced magnetic properties of transition metal and rare-earth metal systems. The new level of performance and the capability of modern computational simulations can help to alleviate the use of many expensive experimental procedures, and can gradually build effective tools to help in the search for new magnetic materials.

2. Magneto-crystalline anisotropy

As suggested by Néel [13], the lack of neighbors and the lowered symmetry at a surface or interface can give rise to the so-called *magnetocrystalline surface anisotropy*. The anisotropy energy at a surface or interface may reach as much as 10^{-3} eV/atom, which is two to three orders of magnitude larger than bulk values. Thus, the demagnetizing energy can be overcome in ultra-thin films, which leads to the spectacular result of spontaneous perpendicular magnetization, as observed experimentally in many cases [14]. As proposed by van Vleck [15] more than 60 years ago, the magnetic anisotropy originates mainly from the SOC interaction among d-states. The SOC Hamiltonian, $H^{soc} = \xi\sigma\cdot\boldsymbol{L}$ (here σ and $\boldsymbol{L}$ are spin and orbital angular momentum operators, respectively), however, is very weak compared to the crystal-field effects. Thus, it has been very difficult to determine E_{MCA} from first-principles calculations, which usually require a large number of k-points and accurate band structures.

Brooks [16], and later Fletcher [17], used an itinerant-electron model to explain the magnetic anisotropy and the quenching of orbital angular momentum in cubic crystals by treating SOC as a perturbation (fourth order for cubic lattices). Because of a rather crude approximation and inaccurate knowledge of the band structure, these authors obtained only a reasonable order of magnitude. Later, Bruno [18] extended this treatment to include the orbital moment (which is largely quenched in transition metals) with the aim of providing qualitative trends. The calculated anisotropy energy, which has a strong connection to the orbital magnetic moment (0.1–0.3 μ_B), depends sensitively on the crystal field and other parameters [19].

Pioneering first-principles calculations of E_{MCA} were carried out by Gay et al. for ferromagnetic Fe, Co, Ni and V monolayers, and thicker Fe slabs and Fe/Ag(0 0 1) [20,21] by incorporating H^{SOC} as a perturbation. In most of ab initio calculations, the MCA force theorem [22–24],

$$E_{MCA} = E(\rightarrow) - E(\uparrow) = \sum_{occ'} \varepsilon_i(\rightarrow) - \sum_{occ''} \varepsilon_i(\uparrow) + O(\delta\rho^n) \quad (1)$$

has been adopted for the determination of E_{MCA}. Here ε_i stands for the band energy of the ith state and the arrows in the parentheses denote the directions of magnetization. Strong numerical uncertainties have been inherent in most previous ab initio MCA calculations because the sets of occupied states, i.e., $\{occ'\}$ and $\{occ''\}$, were determined through the Fermi filling scheme which relies on the very limited information from the eigenvalues, ε_i. One had to use a huge number of k-points ($> 10\,000$ in the two-dimensional Brillouin zone for thin films) to obtain reliable E_{MCA} values and thus only few systems (e.g., free monolayer or simple alloys) can be treated.

2.1. The state-tracking and torque approaches

We proposed a simple solution for this problem by using the state-tracking (ST) approach in which the $\{occ'\}$ and $\{occ''\}$ states are determined according to their projections back to the occupied set of unperturbed states [25,26]. Since this procedure ensures the minimum change in the charge and spin densities, as required by the force theorem, and excludes possible randomness in the Brillouin zone (tracking at a given k-point), very stable MCA results have been obtained with a relatively small number of k-points for magnetic thin films such as Fe, Co and Ni monolayers in the free standing case as well as on various substrates (Cu and Pd, etc).

More recently, we proposed a torque (TQ) method which can further depress the remaining uncertainties resulting from the SOC interaction between near-degenerate states around the Fermi level (the so-called surface pair coupling) [27]. To demonstrate the idea of the torque method, recall that the total energy of an uniaxial system can be well approximated in the form

$$E = E_0 + K_2 \sin^2\theta + K_4 \sin^4\theta. \quad (2)$$

Its angular derivative (torque) is thus

$$T = \mathrm{d}E/\mathrm{d}\theta = \sin(2\theta)[K_2 + 2K_4 \sin^2\theta], \quad (3)$$

where θ is the angle between the normal axis and the direction of magnetization. If we apply the Feynman–Hellman theorem, E_{MCA} can be evaluated finally (note that only $H^{\mathrm{soc}} = \xi\sigma\cdot\boldsymbol{L}$ depends on θ in the Hamiltonian) as

$$E_{\mathrm{MCA}} = \sum_{\mathrm{occ}} < \Psi_i'|\partial H/\partial\theta|\Psi_i' > |_{\theta=45^\circ}$$

$$= \sum_{\mathrm{occ}} < \Psi_i'|\partial H^{\mathrm{soc}}/\partial\theta|\Psi_i' > |_{\theta=45^\circ}, \quad (4)$$

where Ψ_i' is the ith perturbed wave function.

Test calculations for many 3d thin film systems indicate that the MCA energies obtained through $E_{\mathrm{MCA}} = E(\theta = 90^0) - E(\theta = 0^0)$ or through Eq. (4) with state tracking for the band filling are very close to each other (cf. the two thin lines in Fig. 1 for the Ni monolayer with $a = 4.83$ a.u.). The advantage of the torque method is obvious since E_{MCA} is expressed as the expectation value of the angular derivative of H^{soc} and thus it is much more insensitive to distortions of the Fermi surface and only one Fermi surface needs to be determined. In fact, the MCA energies determined through the torque approach with blind Fermi filling (the Torque-FF result for the Ni monolayer is shown as the bold line in Fig. 1) is also very close to those obtained from the state-tracking approach. Since the Torque-FF approach allows relaxation of Fermi surfaces, it is used for the determination of E_{MCA} below.

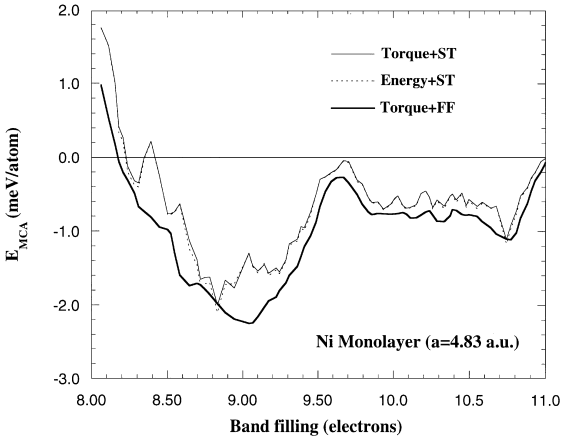

Fig. 1. The calculated E_{MCA} of a free Ni(0 0 1) monolayer ($a = 4.83$ a.u.) versus the band filling (i.e., the number of valence electrons). The thin solid (dashed) line is obtained from torque (energy difference) calculations with the state-tracking method. The bold solid line is obtained from torque with the Fermi filling approach.

Very stable results of E_{MCA} can be obtained through the state-tracking and torque approaches with a reasonable number of k-points (about 200 in the 2D BZ for thin films). This allows us to (1) make explanations and prediction for many magnetic thin films of practical importance; (2) provide physical insights for E_{MCA} from the most fundamental level (e.g., band structure, wave functions and ligand interaction), which was thought to be extremely complex.

2.2. Fe, Co *and* No *monolayers*

As the simplest magnetic systems, free standing Fe, Co and Ni monolayers have been studied

extensively. For example, their calculated E_{MCA} in a square lattice matching the Cu(0 0 1) surface are listed in Table 1. As seen from Fig. 1, the calculated E_{MCA} results are very smooth with respect to the change of band filling (which shows the dependence on occupation number), with either the state-tracking or the torque approach. The data in Table 1 were obtained through Torque-FF calculations with 210 k-points in the two-dimensional irreducible Brillouin zone (BZ).

In their pioneering calculation, Gay and Richter [20,21] obtained $E_{MCA} = 0.61$ meV for the Fe monolayer with the linear combination of atomic orbitals method and 14 400 k-points in the BZ. Using only 15 k-points for the charge density convergence and 66 k-points for the determination of the MCA energy, the state-tracking approach gave 0.42 meV [28] and -1.35 meV [29] of the MCA energy for the Fe and Co monolayers, respectively. Recent tight binding calculations with parameters obtained by a fit to first-principles calculations for Fe and Ni monolayers (rather than their bulks) also got reasonable results (0.17 meV for Fe monolayer and -0.12 for Ni monolayer) [30]. Obviously, E_{MCA} for a given system is sensitive to the treatment of H^{SOC}, the number of k-points and the accuracy of the band structure and wave functions in different approaches.

As described above, the behavior of MCA for transition metal thin films can now be related to more fundamental properties such as band structures and wave functions. This enables us to explore the underlying physics and, furthermore, to figure out a way to tune the MCA for transition metal systems. The k-distributions of the MCA energies and their band structures of Fe, Co and Ni monolayers are plotted in Fig. 2 along the high-symmetry directions in the 2D BZ. Clearly, major E_{MCA} changes happen only when bands cross the Fermi level. Note that SOC interaction between states with the same (different) magnetic quantum number(s), m, is through the $L_z(L_x)$ operator and thus gives a positive (negative) contribution to E_{MCA}.

For the Fe monolayer, the SOC interaction between the occupied d_{z^2} state (at -0.3 eV) and the unoccupied $d_{xz,yz}$ states (at 1.3 eV) results in a negative E_{MCA} (in-plane anisotropy) in the vicinity around the $\bar{\Gamma}$. When the d_{z^2} state becomes unoccupied at $\frac{1}{4}(\bar{\Gamma} - \bar{M})$, the SOC interactions between

Table 1
The calculated spin (M_S, in μ_B) and orbital (M_L, in μ_B) magnetic moments, the anisotropy of orbital moment ($\Delta M_L = \langle L_z \rangle - \langle L_x \rangle$, in μ_B), and the MCA energies (E_{MCA}, in meV/atom) for Fe, Co and Ni monolayers in a square lattice matching the Cu(0 0 1) surface.

System	Method	M_S	M_L	ΔM_L	E_{MCA}
Fe(0 0 1)	FLAPW-GGA	3.04	0.089	0.006	+ 0.50
	FLAPW-LDA	3.00	0.097	− 0.011	+ 0.21
Co(0 0 1)	FLAPW-GGA	2.12	0.236	− 0.096	− 1.49
	FLAPW-LDA	2.09	0.248	− 0.102	− 1.42
Ni(0 0 1)	FLAPW-GGA	1.03	0.185	− 0.057	− 0.77
	FLAPW-LDA	1.00	0.228	− 0.098	− 1.64

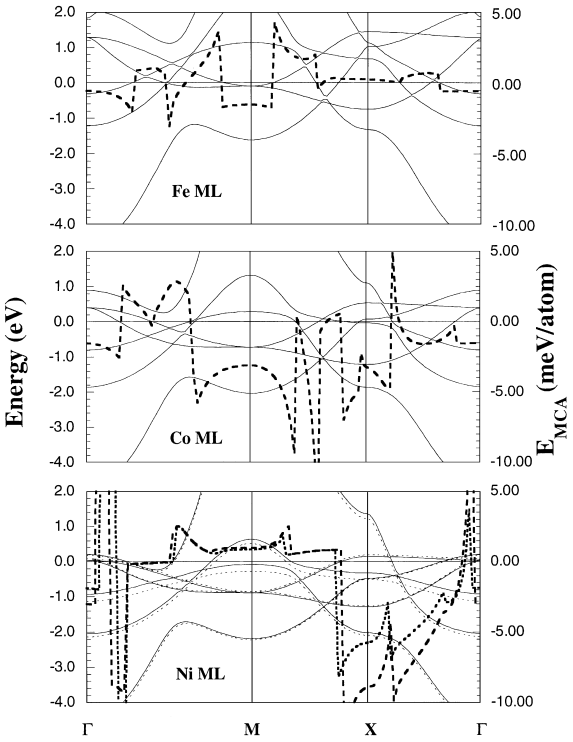

Fig. 2. The LDA band structure (thin lines) and the distribution of E_{MCA} (bold dashed line) along the high-symmetry directions in the 2D BZ for Fe, Co and Ni monolayers in a square lattice ($a = 4.83$ a.u.). In the panel for Ni, the GGA results are given as dotted lines.

the $d_{x^2-y^2}$ and $d_{xy}(m=2)$ states and between the d_{xz+yz} and d_{xz-yz} $(m=1)$ states make positive contributions to the MCA energy in most of the BZ. Around $\bar{M}$, the $d_{(x\pm y)z}$ states lie below E_F; the $d_{x^2-y^2}$ and d_{xy} states are far apart from each other (by 4.5 eV), and the contribution from the SOC interaction between the d_{z^2} (at 1.1 eV) and the $d_{xz,yz}$ (at -0.1 eV) states prevails again – which leads to a negative MCA energy contribution.

For the Co monolayer, the situation is very similar except that the area around $\bar{M}$ with negative MCA energy is enlarged significantly due to a shift of E_F. The intensity of the MCA energy distribution is also strongly enhanced (by a factor of two) since (1) the strength of the SOC in Co atoms ($\xi_{Co}=40$ meV) is much larger than that for Fe atoms ($\xi_{Fe}=32$ meV) and (2) the d-band of Co is about 15–20% narrower than that of Fe. As a result, the Co monolayer has a large negative MCA energy (-1.4 meV/atom). The different sign of MCA energies for Fe and Co monolayers is primarily due to their different band fillings.

The situation for Ni is quite different. The d_{z^2} band is fully occupied in the whole BZ and the vicinity around $\bar{M}$ contributes a positive MCA energy. The large negative MCA energy for the Ni monolayer results mainly from the SOC interaction between the occupied d_{xy} and d_{z^2} states and the unoccupied d_{xz} state along the $\bar{\Gamma}-\bar{X}$ axis.

Although the GGA [31,32] and LDA [33] formulas for the exchange-correlation energy/potential give very close spin magnetic moments for all the three systems, they yield significantly different E_{MCA} results, especially for Ni. For example, as seen in the band structures of the Ni monolayer in Fig. 2, the gradient corrections (dotted lines) appear to shift down the d_{z^2} (by 0.2 eV) and $d_{x^2-y^2}$ and d_{xy} (by 0.05–0.1 eV), while shifting the $d_{xz,yz}$ states up (by 0.05–0.1 eV). This enlarges the energy separation between the d_{xy} and d_{xz} states and thus reduces the SOC interaction between them. As a result, the GGA gives a much smaller value of E_{MCA} than does LDA.

2.3. Magnetic overlayers

The determination of E_{MCA} in various transition metal ultra-thin films has attracted extensive attention in the last decade [34–39]. Since the perpendicular magnetic anisotropy is an important feature for technological applications such as magneto-optical recording [40], it is thus crucial to understand its mechanism. Experimentally, for example, the in-plane easy axis of Co films on Cu(0 0 1), Cu(1 1 0) and Cu(1 1 1) can be turned to the perpendicular direction when they are capped by a few monolayers of nonmagnetic atoms such as Cu, Pd, Ag or Au [35,36]. Weber et al. reported that the magnetic anisotropy of a Co thin film is influenced by the nonmagnetic vacuum/Cu interface even when it is displaced by as much as 16 atomic monolayers from the Co layers [38]. Hope et al. found that a submonolayer Cu coverage can completely reverse the in-plane easy axis when depositing Cu overlayers onto the CO gas dosed Co/Cu(1 1 0) surface [39].

The MCA energies for most systems with lower than cubic symmetry can now be determined quite satisfactorily using various first-principles approaches. To optimize the atomic structures, however, the GGA improves the calculation since LDA is known to significantly underestimate the lattice constants of 3d transition metals. For example, with the in-plane lattice constant fixed ($a=4.83$ a.u.), the optimized Co–Cu interlayer distance in Co/Cu(0 0 1) and Cu/Co/Cu(0 0 1) is 3.44 a.u. from GGA calculations [41], but it is only 3.08–3.11 a.u. if the LDA is adopted [42–45]. The large difference in atomic arrangement may strongly affect all the magnetic properties such as magnetic moments, magnetic ordering and MCA energies.

In Fig. 3, the calculated values of both uniaxial (K_1) and in-plane (K_2) coefficients for Co/Cu(0 0 1), Cu/Co/Cu(0 0 1), and 2Cu/Co/Cu(0 0 1) are given versus a range of their numbers of assumed valence electrons (i.e., band filling).[1] Interestingly, the calculated K_1 changes drastically, from -0.59 meV

[1] For systems with a fourfold symmetry with respect to the surface normal, their magnetic anisotropy energies, E_{MCA}, can be expressed in the lowest nonvanishing order of the polar and azimuth angles (θ and ϕ) as $E_{MCA}=K_1\sin^2\theta+K_2\sin^2(2\phi)\sin^4\theta$, where K_1 and K_2 are coefficients of the leading uniaxial and in-plane contributions, respectively.

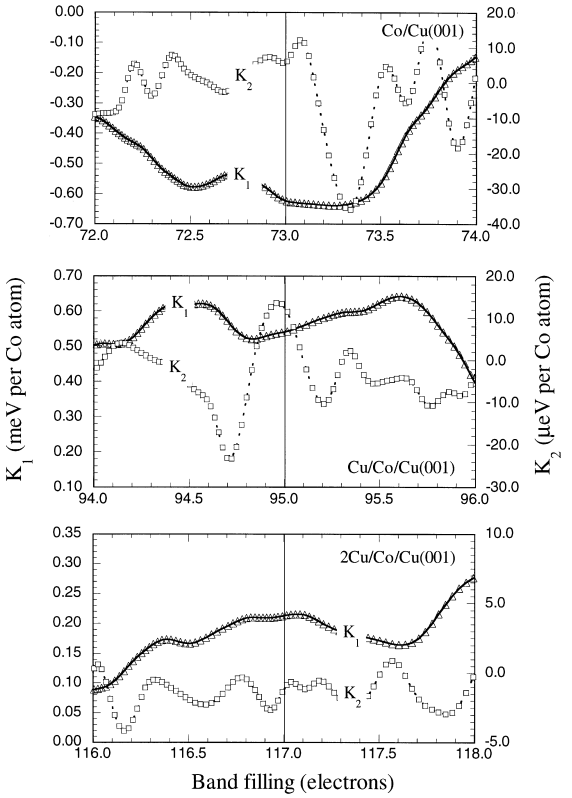

Fig. 3. The E_{MCA} coefficients for the Cu/Co/Cu(0 0 1) systems versus their band fillings.

per Co atom for Co/Cu(0 0 1) to + 0.54 meV per Co atom for Cu/Co/Cu(0 0 1) and, finally, to 0.21 meV per Co atom for 2Cu/Co/Cu(0 0 1). These results agree with the experimental observations by Krams et al. [35] for Cu/Co/Cu(0 0 1) and by Engel et al. [36] for Co films in other structures, in that the nonmagnetic Cu coverage alters the direction of the Co magnetization from in-plane to perpendicular.

Physically, proximity effects of the Cu substrate split the Co-$d_{xz,yz}$ states (cf. Fig. 2) in the low-energy region and enlarge the energy separation between the occupied Co-$d_{xz,yz}$ states and the unoccupied d_{z^2} state around $\bar{M}$. As a result, the negative MCA energy of Co/Cu(0 0 1) is reduced in magnitude (to − 0.61 meV/atom) compared to that for a free Co monolayer (1.42 meV/atom). The additional Cu cap layer enhances the Co/Cu interfacial hybridization (with two interfaces) and thus further weakens the SOC interaction between the Co-$d_{xz,yz}$ and Co-d_{z^2} states. The positive contribution to the MCA energy finally prevails in Cu/Co/Cu(0 0 1) and thus the easy axis of the Co magnetization turns to the perpendicular direction. The second Cu cap layer in 2Cu/Co/Cu(0 0 1), however, indirectly reduces the Co–Cu interfacial hybridization by broadening and shifting the d-band of the first Cu cap layer to the low-energy region. Subsequently, the positive E_{MCA} of 2Cu/Co/Cu(0 0 1) decreases somewhat from that of Cu/Co/Cu(0 0 1) to 0.21 meV per Co.

A simple effective ligand interaction model (ELIM) was developed by Wang et al. [46] to explain effects of interfacial hybridization on the uniaxial E_{MCA} for Cu/Co/Cu surfaces and multilayers. Based on the tight-binding analyses, the E_{MCA} was found to depend on the ratio of vertical and in-plane d-band hybridization. For Co, stronger vertical bonds lead to perpendicular magnetic anisotropy.

Consistent with experiments [35], the calculated values of K_2 are positive for Co/Cu(0 0 1) (6 μeV) and Cu/Co/Cu(0 0 1) (11 μeV), indicating that the easy axis is along the (1 1 0) direction in the cubic unit cell (see foot note 1). In 2Cu/Co/Cu(0 0 1), K_2 changes to negative (− 1 μeV) demonstrating that the in-plane MCA energy is very sensitive to the environment, even to changes in the second nearest neighbors. Krams et al. [35] found the K_2 coefficient to be almost independent of the Cu coverage, but more recent experiments by Weber and Hope et al. [38,39] observed significant changes in K_2 with Cu coverage, even when it is as thick as 16 monolayers.

Table 2 gives the calculated and measured E_{MCA} for several selected magnetic thin films. Using the state-tracking approach and an unrelaxed atomic structure (UR), Wang et al. [46] obtained MCA energies of − 1.35, − 0.38 and − 0.01 meV for Co monolayer, Co/Cu(0 0 1) and the Cu/Co/Cu sandwich. By including the SOC Hamiltonian into the self-consistent iterations for one direction of magnetization, and using the force theorem for rotation to determine E_{MCA}, Shick et al. [44,45] obtained $E_{MCA} = -0.395$ meV for Co/Cu(0 0 1) and $E_{MCA} = -0.70$ meV for Cu/Co/Cu(0 0 1) with a fully relaxed structure through FLAPW-LDA

Table 2
Calculated MCA energies for selected transition magnetic thin films

System	Method	E_{MCA}
Co/Cu(0 0 1)	FLAPW-LDA-ST-UR [46]	− 0.38
	FLAPW-LDA-SC-RL [44,45]	− 0.36
	FLAPW-LDA-ST-RL [42,43]	− 0.09
	FLAPW-GGA-TQ-RL [41]	− 0.61
	SKKR-LDA-UR [47]	− 0.38
	Experiment [35]	− 0.37
Cu/Co/Cu(0 0 1)	FLAPW-LDA-ST-UR [46]	− 0.01
	FLAPW-GGA-TQ-RL [41]	+ 0.54
	SKKR-LDA-UR [48]	+ 0.85
	Experiment [35]	+ 0.1
Co/Cu(1 1 1)	FLAPW-LDA-ST-RL [48]	− 0.30
Co/Pd(0 0 1)	FLAPW-LDA-ST-RL [76]	− 0.91
Co/Pd(1 1 1)	FLAPW-LDA-ST-RL [76]	+ 0.25
Pd/Co/Pd(0 0 1)	FLAPW-LDA-ST-UR [118]	+ 0.56
Ni/Cu(0 0 1)	FLAPW-LDA-ST-UR	− 0.69
2Ni/Cu(0 0 1)	FLAPW-LDA-ST-UR	+ 0.33
3Ni/Cu(0 0 1)	FLAPW-LDA-ST-UR	+ 0.08
4Ni/Cu(0 0 1)	FLAPW-LDA-ST-UR	− 0.06
Cu/Fe/Cu(0 0 1)	SKKR-LDA [119]	− 0.41
	LMTO-LDA [120,121]	− 0.43
Fe/Au(0 0 1)	FLAPW-LDA [122]	+ 0.57
	SKKR-LDA [123]	+ 0.56

calculations. In Co/Cu(0 0 1), the SOC in Cu atoms is found to give an opposite contribution (0.045 meV) to E_{MCA} than does that in Co (-0.440 meV). In recent model calculations, Szunyogh et al. [47] studied the effects of different caps and identified a correlation of E_{MCA} with some features in the electronic properties of the Co and the cap layers. Zhong et al. [48] and Kim et al. [49] also studied the effects of the Cu cap layers on the E_{MCA} of Co/Cu(1 1 1) and Co/Cu(1 1 0). Similar to the Co/Cu(0 0 1) case, E_{MCA} is -0.30, $+0.30$ and -0.02 meV for Co/Cu(1 1 1), Cu/Co/Cu(1 1 1) and 2Cu/Co/Cu(1 1 1), respectively [48].

Very recently, the symmetry induced E_{MCA} in striped magnetic films or vicinal magnetic surfaces has attracted great attention. A striking sensitivity of the easy magnetization axis was found in epitaxial stepped Co films with changes of step density and cap (Cu) coverage [50,51]. Zhong et al. carried out model FLAPW-ST calculations for ultrathin striped Co films, with and without Cu decoration [52], and found a 90° in-plane spin reorientation by the Co decoration. A useful expression of E_{MCA} versus the vicinal angle was recently developed by Shick et al. [53] based on Néel's model and discussed by Kawakami et al. [54–56] with experimental data for various stepped surfaces.

2.4. Cubic magnetic bulks

The first-principles determination of E_{MCA} in cubic bulk magnetic Fe, Co and Ni is one of the longest standing challenging problems in condensed matter physics. Due to the high symmetry, E_{MCA} in these cubic systems is extremely small – only about 1 μeV/atom. Quantitatively, such a scale of energy difference is very close to or beyond the limit of precision of total energy calculations for most approaches. Early calculations with the force theorem repeatedly gave the wrong sign for either Fe or Ni (or both). Using the LMTO-ASA approach, Daalderop et al. [57] obtained the right magnitude of E_{MCA}, but the wrong easy axis for HCP Co and FCC Ni. Guo et al. [58] and Strange et al. [59] also obtained the wrong easy axis or wrong magnitude for bulk Fe and Ni in their LMTO and KKR calculations. Based on the full potential LMTO method, Trygg et al. [60] treated the SOC Hamiltonian self-consistently but obtained (with *spd*-basis functions) almost the same results as Daaderop et al. The accuracy of total energy calculations was re-examined by Halilov et al. [61], also using the LMTO-ASA method with combined corrections. They obtained the correct easy axis for all three metals through total energy calculations with a larger set of k-points. Beiden et al. [62] implemented a real-space locally self-consistent multiple scattering method. Again, they obtained the wrong easy axis for Ni and oscillatory results for HCP Co.

We extended the torque method for the determination of E_{MCA} in cubic crystals, where the total energy can be well approximated in the form

$$E = E_o + K_1(\alpha_1^2\alpha_2^2 + \alpha_1^2\alpha_3^2 + \alpha_2^2\alpha_3^2) + K_2\alpha_1^2\alpha_2^2\alpha_3^2. \quad (5)$$

Here α_1, α_2 and α_3 are directional cosines referred to the cubic edges along the x, y and z axes. Clearly, the E_{MCA} can be evaluated from the coefficients of

K_1 and K_2 as

$$E_{111} - E_{001} = \frac{K_1}{3} + \frac{K_2}{27}, \quad E_{110} - E_{001} = \frac{K_1}{4}. \tag{6}$$

As in Eq. (3) for thin films, the torque here, $T(\theta)$, is defined as the derivative of the total energy with respect to the polar angle away from the z-axis (denoted as θ below). To determine the values of K_1 and K_2, we focus on two special cases: (1) for $\alpha_2 = 0 (\alpha_1^2 = 1 - \alpha_3^2)$, we have

$$T_1(\theta) \equiv \frac{\mathrm{d}E(\theta)}{\mathrm{d}\theta}|_{\phi=0^\circ} = \frac{K_1}{2}\sin(4\theta) \tag{7}$$

and (2) for $\alpha_1 = \alpha_2 (\alpha_1^2 = \alpha_2^2 = (1 - \alpha_3^2)/2)$

$$T_2(\theta) \equiv \frac{\mathrm{d}E(\theta)}{\mathrm{d}\theta}|_{\phi=45^\circ} = T_1(\theta) + \frac{\sin(2\theta)\sin^2(\theta)}{4} \times [2K_1 + K_2(3\cos^2\theta - 1)], \tag{8}$$

where ϕ denotes the azimuzal angle in the xy plane. We have

$$T_1(\theta = 22.5^0) = K_1/2, \quad T_2(\theta = 45^0) = (2K_1 + K_2/2)/8 \tag{9}$$

and finally the MAE coefficients K_1 and K_2 can be evaluated very efficiently through

$$K_1 = 2T_1(\theta = 22.5^0), \quad K_2 = 16T_2(\theta = 45^0) - 4K_1. \tag{10}$$

The calculated K_1 and K_2 for BCC Fe with the FLAPW-GGA-TQ approach are given in Fig. 4. While K_1 is found to be still oscillatory but stable in sign with $70 \times 70 \times 70$ k-points in the full BZ for the cubic cell (with two atoms), K_2 changes its sign very rapidly. It appears that more k-points are needed to get a converged result for K_2. Fortunately, K_2 remains very small and does not affect the anisotropy energy too much (cf., the $\frac{1}{27}$ scaling factor in Eq. (6) for $E_{111} - E_{001}$). The calculated E_{MCA} $(E_{111} - E_{001})$ for BCC bulk Fe is 0.9 (0.7) μeV/atom with GGA (LDA) formula (the (0 0 1) direction is the easy axis). The LDA value is very close to the results obtained by Daalderop et al. (0.5 μeV/atom, with the force theorem) [57], Trygg et al. (0.5 μeV/atom, with total energy) [68] and Beiden et al. (0.78 μeV/atom, with a real space approach). The discrepancy between theory (0.5–0.9 μeV/atom) and experiment (1.4 μeV/atom) appears not to be due to numerical problems, but to other physical reasons such as possible orbital polarization [60,63,64].

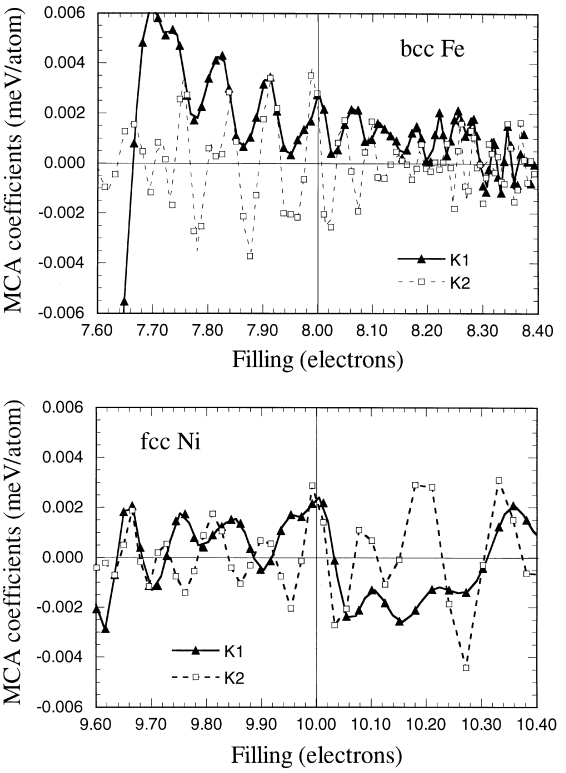

Fig. 4. The E_{MCA} coefficients of BCC bulk Fe ($a = 5.41$ a.u.) and FCC bulk Ni ($a = 6.66$ a.u.) versus their band fillings.

For FCC Co and Ni, the calculated E_{MCA} results with the FLAPW-TQ approach are also very close to those obtained in previous density functional calculations. With $50 \times 50 \times 50$ k-points in the full BZ for the cubic cell (with four atoms), the correct easy axis is obtained for Co, but not for Ni. In addition, the theoretical E_{MCA} results are much smaller in magnitude than the experimental data. The failure of the density functional description for E_{MCA} in bulk FCC Ni appears to be mainly due to s–d charge transfer. Note that with $a = 6.66$ a.u., the calculated spin magnetic moments of Ni are 0.62 and 0.67 μ_B with LDA and GGA, respectively. These values are markedly larger than the experimental result, 0.57 μ_B. Since the spin magnetic

moment in Ni is almost equal to the number of holes in its minority spin d-band, this discrepancy indicates that the Ni-d band has about 0.05–0.10 fewer electrons than what it should have. Such an error in band filling is enough to change the sign of E_{MCA}. As shown in Fig. 4, K_1 and K_2 could become negative by moving only 0.03 electrons from the Ni s-band to its d-band.

3. Magnetostriction

3.1. General equations

In general, the size of the magneto-elastic strain induced by rotation of the magnetization depends on the directions of the measured strain and of the spin moment with respect to the crystalline axes of the material. For a cubic material, the directional dependence of the fractional change in length can be expressed in terms of the direction cosines of the magnetization (α_i) and of the strain measurement direction (β_i) with respect to the crystalline axes [65]:

$$\frac{\Delta l}{l_0} = \frac{3}{2}\lambda_{001}\left[\sum_{i=1}^{3}\alpha_i^2\beta_i^2 - \frac{1}{3}\right] + 3\lambda_{111}\sum_{i\neq j}^{3}\alpha_i\alpha_j\beta_i\beta_j. \quad (11)$$

If the measurement is carried out along the (0 0 1) direction for example, $\beta_x = \beta_y = 0$ and $\beta_z = 1$, then Eq. (11) can be simplified as $\frac{\Delta l}{l_0} = \frac{3}{2}\lambda_{001}\left[\alpha_z^2 - \frac{1}{3}\right]$ or further, for systems with a single domain

$$\lambda_{001} = \frac{2}{3}\frac{l_0(\alpha_z = 1) - l_0(\alpha_z = 0)}{l_0(\alpha_z = 1)}. \quad (12)$$

Clearly, λ_{001} represents the change in length along (0 0 1) when the magnetization turns from the x, y plane to the z direction.

The equilibrium length along the z direction, l_0, can be obtained by fitting the calculated total energy as a quadratic function of l:

$$E(\alpha_z = 1) = al^2 + bl + c, \quad E(\alpha_z = 0) = E(\alpha_z = 1) + E_{MCA}(l) \quad (13)$$

and so

$$\lambda_{001} = -2E'_{MCA}/3b. \quad (14)$$

Here $E'_{MCA} = dE_{MCA}/dl$, which is much smaller than the value of b. Note that b is always negative (since both a and l_0 are positive), and thus λ and E'_{MCA} have the same sign.

3.2. Cubic magnetic bulks

As an important benchmark test, the magnetostriction coefficients of cubic bulk magnetic transition metals are studied first. The calculated MCA energy is found to be a smooth monotonic function of the vertical strain. The slope of E_{MCA} and thus the magnetostrictive coefficient (λ_{001}) are positive for Fe and Co but negative for Ni. This means that bulk Fe and Co (Ni) stretch (shrink) along the direction of magnetization, a conclusion that agrees well with experiment.

Quantitatively, the value of λ_{001} depends sensitively on the distortion mode (i.e., Poisson's ratio). As listed in Table 3, the value of Poisson's ratio for Fe, Co and Ni optimized through total energy minimization is about 0.40, which is very close to that obtained using the measured elastic stiffness constants ($\sigma = -c_{12}/(c_{11} + c_{12})$) for bulk Fe and Ni (0.37–0.38). As a result, satisfactory quantitative agreement is achieved for λ_{001} between our (zero temperature) theory and experiment.

Table 3
Calculated equilibrium lattice constants a (in a.u.), Poisson's ratio (σ), spin and orbital magnetic moments (M_S and M_L, in μ_B), $E_{111} - E_{001}$ (E_{MCA}, determined with the experimental lattice constants, in μeV) and magnetostriction coefficients (in 10^{-6}) obtained with LDA and GGA corrections

	a	σ	M_S	M_L	E_{MCA}	λ_{001}
BCC Fe						
LDA	5.20	−0.409	2.05	0.048	0.7	52
GGA	5.37	−0.486	2.17	0.045	0.9	29
EXP	5.41	−0.368	2.22	0.08	1.4	21
FCC Co						
LDA	6.48	−0.374	1.59	0.076	—	92
GGA	6.67	−0.396	1.66	0.073	−0.6	56
EXP	6.70	—	1.72	—	−1.8	79
FCC Ni						
LDA	6.46	−0.332	0.62	0.049	0.7	−63
GGA	6.64	−0.376	0.66	0.050	0.8	−56
EXP	6.66	−0.376	0.57	0.05	−2.7	−49

The theoretical result can be further improved by using the GGA [31,32]. As seen in Table 3, LDA leads to a 3% underestimation for the lattice constant and a more substantial difference for the spin magnetic moments at the equilibrium geometry. With GGA, most of the calculated values of the various magnetic properties are closer to experiment, especially for Fe in which the number of holes with majority spin is very sensitive to the change of environment.

The inverse effect of magnetostriction is strain-induced uniaxial E_{MCA} in thick epitaxial magnetic films. This effect is believed to play a key role for the spin reorientation of Ni/Cu(0 0 1) when the Ni film becomes thicker than 7 layers [66]. We calculated the volume contribution to the MCA energies of Ni films from FCT bulk Ni with the fixed lateral lattice constant of the Cu(0 0 1) substrate ($a = 6.831$ a.u.) [67]. The E_{MCA} is found to be a linear function of the lattice distortion along the c-axis. When the measured length of the c-axis ($l = 6.43$ a.u.) is adopted, the calculated MCA energy is $+65\,\mu$eV/atom. This result agrees vary well with experiment, which gave $E_{MCA} = +70\,\mu$eV/atom extrapolated to zero temperature [68,69].

Using the FLMTO approach, Hjortstam et al. [70] obtained a value of $60\,\mu$eV/atom for the strain-induced E_{MCA}. More recent FLAPW calculations by Shick et al. (by treating SOC self-consistently for one spin direction and using the force theorem for rotation) obtained $E_{MCA} = 57\,\mu$eV/atom for FCT Ni [53]. If the surface/interface contributions to E_{MCA} is taken from Ni/Cu(0 0 1) in Table 2 ($-690\,\mu$eV/atom), one may conclude that the in-plane to perpendicular spin-reorientation transition occurs at a thickness of 10–11 Ni-layers, a result which agrees reasonably with experiment (7 Ni-layers) [68,69].

If the orbital polarization is included, Hjortstam et al. [70] obtained $E_{MCA} = 140\,\mu$eV/atom for FCT Ni. They also gave a very large magnetostrictive coefficients for FCT Ni, $\lambda_{001} = -270 \times 10^{-6}$ and $\lambda_{111} = -107 \times 10^{-6}$, which are almost three times larger in magnitude than experiment [71–73], $\lambda_{001} = -71 \times 10^{-6}$ and $\lambda_{111} = -39 \times 10^{-6}$. Thus, it appears that the orbital polarization term, while improving the calculated orbital magnetic moments, overcorrects the SOC far too much for the determination of E_{MCA}. By contrast, our recent FLAPW-GGA-SOC calculations obtained $\lambda_{001} = -71 \times 10^{-6}$ and an equilibrium length of the c-axis of $l_0 = 6.43$ a.u.; both results are in excellent agreement with experiment.

3.3. Fe, Co and Ni alloys

Ni_xFe_{1-x} and Ni_xCo_{1-x} magnetic alloys are widely used in magnetic recording technology and invar materials. Despite the fact that their magnetic properties are being studied in great detail both experimentally and phenomenologically [74], there is no microscopic theoretical description of the magnetic anisotropy and magnetostriction for these systems. We carried out a series of investigations for the magnetostriction in FeNi and CoNi alloys through FLAPW-GGA calculations.

As listed in Table 4, the optimized lattice constants, elastic constants and magnetic properties agree very well with experiment [75]. Both the $FeNi_3$ and $CoNi_3$ alloys have the cubic $L1_2$ structure and a very small E_{MCA} (since the x and z axis are identical). By contrast, the cubic symmetry is broken in the FeNi and CoNi alloys, which thus have a uniaxial E_{MCA} as large as 63 and 143 μeV/cell, respectively. FeNi adopts the cubic $L1_0$ geometry, while the c-axis of CoNi is 2.4% bigger than its a-axis. The calculated spin magnetic moments of Fe, Co and Ni atoms are very close to the corresponding experimental data.[2]

To calculate the magnetostrictive coefficients, the length of the c-axis is used as a parameter. The E_{MCA} appears to be a smooth function of the lattice strain for each system studied. For instance, the calculated total energy and MCA energy for $FeNi_3$ are plotted in Fig. 5 versus the lattice distortion along the z-axis (c_0 is 6.66 a.u.; the minimum-energy distortion mode is adopted here [76]). The calculated magnetostrictive coefficient from the curvature of the total energy curve and the slope of

[2] Note that the spin dipolar term, $\langle T_z \rangle$, is quite large in FeNi and CoNi alloys and so one must take this into account when using the magnetic circular dichroism (MCD) sum rules to determine the spin magnetic moments for these systems.

Table 4
Calculated lattice constants a (in plane, in a.u.) and c (along z in a.u.), magnetic moments (M, in μ_B), the Poisson ratio (σ), magnetocrystalline anisotropy energy (E_{MCA}, in μeV/cell) and magnetostriction coefficient ($\lambda_{0\,0\,1}$, in 10^{-6}). The corresponding experimental data are given in parentheses

	FeNi	$FeNi_3$	CoNi	$CoNi_3$
a	6.76(6.76)	6.70(6.71)	6.62(6.67, a & c)	6.66(6.65)
c	6.76(6.76)	6.70(6.71)	6.78	6.66(6.65)
E_{MCA}	63	0	143	0
C_{11}	328	275	318	269
C_{12}	159	151	167	154
σ	− 0.33	− 0.354	− 0.344	− 0.364
λ_{001}	9.7(10–26)	23(12)	32 (42–100)	33
M_S(Fe, Co)	2.71(2.54)	2.95(2.97)	1.75(1.70)	1.76(1.83)
M_L(Fe, Co)	0.052	0.055	0.086	0.105
T_z(Fe, Co)	0.065	0.0	− 0.012	0.0
M_S(Ni)	0.69(0.73)	0.68 (0.68)	0.70 (0.58)	0.70(0.58)
M_L(Ni)	0.038	0.041	0.043	0.045
T_z(Ni)	− 0.006	0.00	− 0.003	0.0
H_{FC}(Fe, Co)	305(306)	237(292)	233	200
H_{FC}(Ni)	334	222	230	179

the E_{MCA} curve is 23×10^{-6} for $FeNi_3$, a value which is much larger than the measured results for an $Fe_{30}Ni_{70}$ polycrystalline sample, 13×10^{-6} [75]. The measured data, however, strongly depend on the temperature and composition. The calculated magnetostrictive coefficients for FeNi and CoNi agree well with experiments [75].

The E_{MCA} for permalloy ($Fe_{20}Ni_{80}$) are also given in Fig. 5. Note that these results are obtained from the $FeNi_3$ band structure using a rigid band model; they thus reflect only the effects of a change of composition (or more exactly, the change of number of valence electrons in the unit cell). The calculated magnetostrictive coefficient for this pseudo-permalloy (11.7×10^{-6}) is much smaller than that of the $FeNi_3$ crystal. Experimentally, it is known that the magnetostrictive coefficient of permalloy is close to zero. The change in number of valence electrons certainly plays a very important role in weakening the magnetostriction.

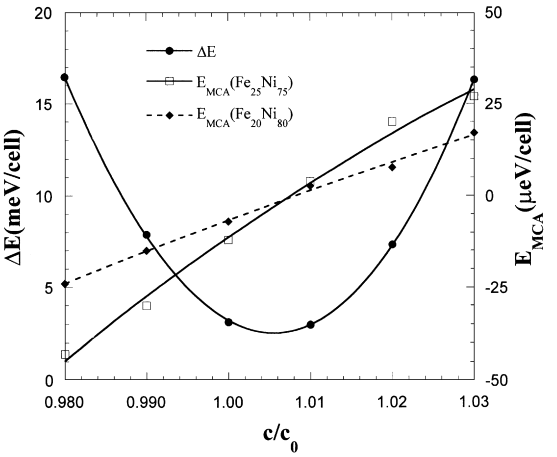

Fig. 5. The calculated total energy and E_{MCA} of $FeNi_3$ versus the lattice strain along the vertical axis. The minimum energy distortion mode is adopted.

3.4. Rare-earth intermetallic compounds

Rare-earth intermetallic compounds have attracted great attention since the late 1960s due to their extraordinary magnetic properties, especially their large magnetostrictive coefficients (10^{-3}) at room temperature [65,77,78]. While it was believed that the localized rare-earth 4f states play a dominant role in magnetization and magneto-elastic coupling, recent experiments found that the effects of itinerant states can be equally important [65,79]. Although a phenomenological approach was developed long ago to describe the dependence of

single crystal magnetostriction on magnetization and measurement directions, the magnetostrictive coefficient for a given material, especially the contribution of itinerant electrons, has never been accurately calculated [65].

Very recently, we investigated the magnetostrictive properties of two prototype rare-earth intermetallic compounds, namely, $GdCo_2$ and $GdFe_2$ [80]. Both compounds adopt the C15 cubic Laves phase structure, a close-packed arrangement of spheres with two different sizes. Through total energy minimization, the calculated equilibrium lattice constants for $GdCo_2$ and $GdFe_2$ are 13.65 and 13.85 a.u., respectively. These values agree very well with their experimental counterparts, 13.69 and 13.94 a.u. [78] – indicating the validity and accuracy of our local density FLAPW calculations for these compounds. As expected, the calculated atomic forces on all the atoms are zero in a range of $\pm$ 2.5% lattice expansion/compression. Thus the C15 cubic Laves phase is a very stable structure for these materials.

As listed in Table 5, the spin magnetic moment for Gd is 7.46 μ_B (7.0 μ_B from the 4f shell and 0.45 μ_B from the valence band) in $GdCo_2$, while it is enhanced to 7.58 μ_B (0.58 μ_B from the valence band) in $GdFe_2$. For both systems, the orbital magnetic moment of Gd remains very small (0.021–0.025 μ_B). In agreement with experiment, the magnetic moments of Co and Fe align anti-parallel to that of Gd. The spin and orbital magnetic moments of the Co atom in $GdCo_2$ are -1.24 and -0.11 μ_B, respectively. The calculated total magnetic moment (spin and orbital parts, including contributions from the interstitial region) for $GdCo_2$ is 4.99 μ_B, a value which agrees very well with experiment (4.9 μ_B) [78]. For $GdFe_2$, the calculated spin and orbital magnetic moments in the Fe sphere are -1.96 and -0.046 μ_B, respectively. The calculated total magnetic moment for $GdFe_2$ at zero temperature, 3.85 μ_B, is significantly larger than the experimental value, 2.80 μ_B. The reason for this large discrepancy is unclear.

To obtain the magnetostrictive coefficients, we applied several different strains along the z-axis with the volume of the unit cell fixed. The calculated total energies (ΔE) and E_{MCA} are plotted in Fig. 6 versus the length of the unit cell along the z-axis, l. The total energy for each system can be well fitted by a third-order polynomial but not by a parabola – indicating the importance of nonlinear elasticity in these materials. The calculated elastic stiffness constants, also listed in Table 5, show that $GdFe_2$ is significantly harder than $GdCo_2$.

The calculated E_{MCA} in Fig. 6 is also a monotonic smooth function of l for each system. Interestingly, the strain dependence of E_{MCA} in $GdCo_2$ behaves very differently from that in $GdFe_2$, and depends sensitively on lattice strain. The large negative slope of the E_{MCA}–l curve indicates that $GdCo_2$

Table 5
Calculated lattice constants (l_0, in a.u.), elastic stiffness constants (c_{11} and c_{12}, in GPa), magnetostrictive coefficients (λ_{001}, in 10^{-6}), and spin (M, in μ_B) and orbital (L_z, in μ_B) magnetic moments of $GdFe_2$ and $GdCo_2$. Data in parentheses are the corresponding experimental results

	$GdFe_2$		$GdCo_2$	
l_0	13.85 (13.94)		13.65 (13.69)	
c_{11}	326		218	
c_{12}	206		147	
λ_{001}	44 (39)		-327 (-1200)	
	Gd	Fe	Gd	Co
M	7.58	-1.96	7.46	-1.24
L_z	-0.021	-0.046	-0.025	-0.110

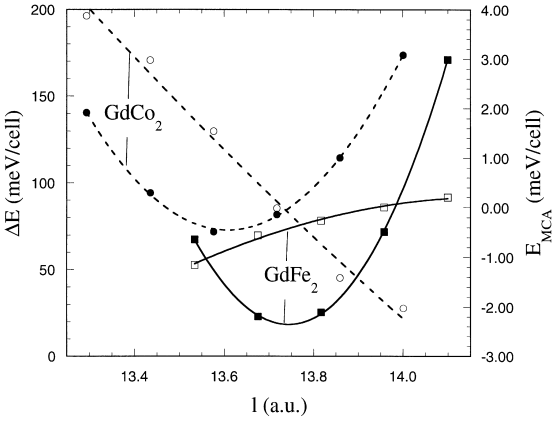

Fig. 6. The calculated total energy and E_{MCA} of $GdFe_2$ (solid lines) and $GdCo_2$ (dashed lines) versus the length of the vertical axis. A constant-volume mode is adopted for the distortion.

contracts along the direction of magnetization. Quantitatively, the value of Δl due to the change of magnetization direction, i.e., $(l(\alpha_z = 1) - l(\alpha_z = 0)$, is -6.69×10^{-3} a.u./cell, or -0.049% of the equilibrium lattice constant ($l_0 = 13.65$ a.u.). The calculated λ_{001} is -327×10^{-6}. While this value is much larger than the magnetostrictive coefficients for magnetic transition metals ($20–70 \times 10^{-6}$), it is still considerably smaller than the experimental value of -1200×10^{-6} [65]. The discrepancy is possibly due to effects of (i) dipole–dipole interactions among the giant Gd magnetic moments, (ii) defects and impurities in the experimental specimens and (iii) the difference in temperature.

By contrast, the strain dependence of E_{MCA} in $GdFe_2$ is much weaker and, significantly, the slope of the E_{MCA}–l curve becomes positive. The calculated magnetostrictive coefficient for $GdFe_2$ is thus positive, $+44 \times 10^{-6}$, and very close to experiment, $\lambda_s = +39$ [77]. Using a rigid band picture, we found that the difference in the magnetostrictive behaviors of $GdFe_2$ and $GdCo_2$ is mainly due to the change in band filling. A $GdFe_xCo_{2-x}$ compound ($x = 0.9–1.2$) is predicted to be a strong magnetostrictive material with a positive sign for $\lambda_{001}(+450 \times 10^{-6})$.

4. Magneto-optical effects

4.1. MOKE

The MOKE is now a widely used in situ tool for studies of magnetic properties of thin films and surfaces [81]. It is known that the MOKE is induced by the SOC interaction among the d-states. In the polar geometry, the Kerr rotation angle, θ_{K}, and ellipticity, ε_{K}, can be expressed as

$$\theta_{\mathrm{K}} + \mathrm{i}\varepsilon_{\mathrm{K}} = \frac{-\sigma_{xy}}{\sigma_{xx}\sqrt{1 + (4\pi\mathrm{i}/\omega)\sigma_{xx}}}, \tag{15}$$

where the diagonal (σ_{xx}) and off-diagonal (σ_{xy}) elements of the optical conductivity tensor can be evaluated by means of the Kubo–Greewood linear response theory [82] as

$$\sigma_{\alpha\beta} = \frac{-\mathrm{i}e^2}{m^2\hbar\Omega}\sum_{\boldsymbol{k}}\sum_{mn}\frac{f_m - f_n}{\omega_{mn}}\frac{\boldsymbol{\Pi}^{\alpha}_{nm}(\boldsymbol{k})\boldsymbol{\Pi}^{\beta}_{mn}(\boldsymbol{k})}{\omega - \omega_{mn} + \mathrm{i}\delta}. \tag{16}$$

Here f_m is the Fermi function, ω_{mn} is the energy difference ($\hbar\omega_{mn} = \epsilon_m - \epsilon_n$) and $\Pi^{\alpha}_{nm}(\boldsymbol{k})$ is the momentum matrix element.

Following the pioneering work of Wang and Callaway [83], MOKE spectra can now be calculated with quite satisfactory results with several first-principles approaches [84]. Prototype studies for bulk Fe, Co and Ni have been recently reported by many groups with basically similar results [85–90]. Theoretical calculations have been performed for many different kind of materials such as compounds, Heusler alloys, surfaces and multilayers [91–94]. To describe the strong correlation effects, the LDA + U scheme is usually employed when rare-earth and actinide elements are involved [95,96]. In general, Kerr rotation spectra vary with composition in a rather complex and unforeseeable way, even for simple systems like Co–Ni alloys. Therefore, the first-principles calculations are essential to explain the measured MOKE spectra.

As an example of the current state of MOKE investigations, we have studied MOKE spectra of several systems such as magnetic bulk transition metals [96], PtFe alloys, Co/Pt thin films and overlayers [97] and FeAu multilayers [98]. In Fig. 7, we present the FLAPW-calculated MOKE spectra for the Fe_3Au_3 multilayer. For the case with a sharp interface, both the amplitude and shape of the calculated MOKE spectra differ markedly from the experimental data [99,100]. We attributed the discrepancy to possible interfacial interdiffusion. Indeed, agreement is improved significantly when two FeAu intermixed layers (we assumed a $c(2 \times 2)$ structure in the lateral unit cell) are introduced in the interfacial region.

For Cu(0 0 1) and Co(1 1 1) thin films [97], the surface effects induce a red-shift for the high-energy peak and reduce the Kerr rotation angle in the low-energy region due to the narrowed bandwidth and enhanced magnetization. In $CoPt_n$ alloys ($n = 1$ and 3), the increase of Pt composition with respect to the CoPt layered alloy reduces the amplitude of the MOKE spectra for the $CoPt_3$ multilayer, whereas it results in a different structure of the MOKE spectra for the $CoPt_3$ alloy. This structural dependence is found to be hardly explained by the change of Pt SOC strength and its effect on the MOKE, even though the large MOKE spectra of

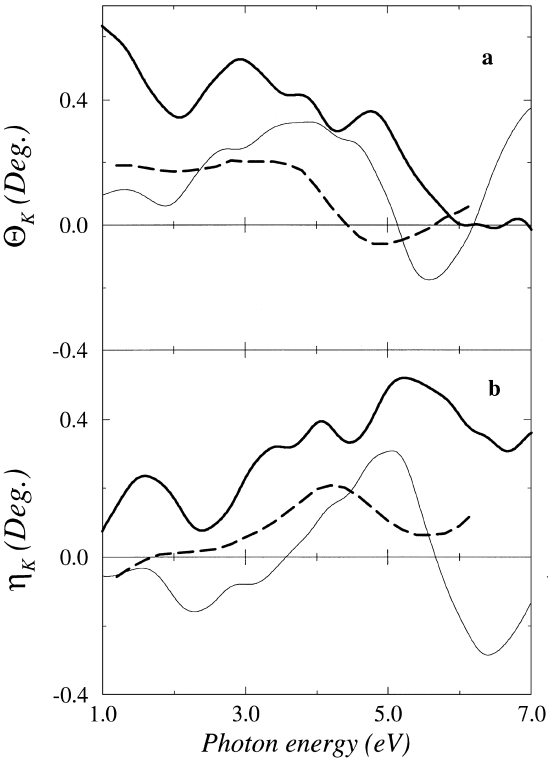

Fig. 7. The calculated spectra of (a) Kerr rotation and (b) ellipticity of the Fe_3Au_3 multilayers. Bold (thin) line is for the case with sharp (intermixed) interfaces. Dashed line is the experimental result.

the CoPt compounds has been mainly attributed to the large Pt SOC strength.

Stimulated by interesting experimental observations by Weller et al. [101,102], several groups have paid close attention to the anisotropy of MOKE in HCP bulk Co, CoPt and FePt alloys and compounds [103–105]. From our recent FLAPW-LDA calculations [97], we found that the anisotropy of the MOKE spectra for bulk Co is negligible for either (0 0 1) or (1 1 1) magnetization direction. For FePt, we found the correct trend of the MOKE spectra for both (1 1 0) and (0 0 1) magnetizations, but large amplitudes (1.1 degree in maximum) [106].

4.2. Magnetic circular dichroism

The possibility to determine both the orbital and spin moments (denoted as $\langle S_z\rangle$ and $\langle L_z\rangle$, respectively) directly from X-ray MCD [107,108] spectra by applying recently proposed simple but powerful sum rules has attracted considerable excitement and attention [109,110]. As stated in the MCD sum rules, integrations of the MCD and total absorption spectra relate directly to $\langle L_z\rangle$, $\langle S_z\rangle$ and $\langle T_z\rangle$ for the unoccupied states

$$\frac{I_m = \int_{L_3+L_2}\sigma_m \,\mathrm{d}E}{I_t = \int_{L_3+L_2}\sigma_t \,\mathrm{d}E} = \frac{\langle L_z\rangle/2}{N_h = \int\rho(E)\,\mathrm{d}E} \tag{17}$$

and

$$\frac{I_s = \int[\sigma_s = \int(\sigma_{m,L_3} - 2\sigma_{m,L_2})]\,\mathrm{d}E}{I_t = \int_{L_3+L_2}\sigma_t \,\mathrm{d}E}$$

$$= \frac{\langle S_e\rangle = (\langle S_z\rangle + 7\langle T_z\rangle)/3}{N_\mathrm{h}}, \tag{18}$$

where $\sigma_m = \sigma_+ - \sigma_-$ and $\sigma_t = \sigma_+ + \sigma_- + \sigma_z$. $\boldsymbol{T}$ is the spin magnetic dipole operator, i.e., $\boldsymbol{T} = \frac{1}{2}[\boldsymbol{S} - 3\hat{r}(\hat{r}\cdot\boldsymbol{S})]$, $(T_z = S_z(1 - 3\cos^2\theta)/2$ for $\boldsymbol{S}$ aligned along the z direction). The number of valence holes, N_h, can be obtained from an integration over the unoccupied density of states ($\rho(E)$).

We carried out first-principles calculations to check the validity and applicability of the sum rules for transition metal systems [111–113]. As listed in Table 6, the deviation of the spin and orbital sum rules is denoted by $R_1 = I_m/I_t/\langle L_z\rangle/N_\mathrm{h} - 1$, and $R_2 = I_s/I_t/\langle S_e\rangle/N_\mathrm{h} - 1$. Obviously, the orbital sum rule is seen to work very well (within 10%) for Fe and Co systems, and the error becomes larger for Ni since the number of s, p holes is almost equal to that of d holes (we used an energy cutoff of 6 eV above E_F). By contrast, the errors of the spin sum rule are much larger: it actually fails severely for the Ni surface since R_2 is as large as 52%. A better way is to combine the $\langle L_z\rangle$ and $\langle S_z\rangle$ sum rules, as was done recently in some experiments on bulk transition metals [114]. From our first-principles calculations, we found that the error in the ratio $R_3 = I_m/I_s/\langle L_z\rangle/\langle S_e\rangle - 1$, is 10% or so for all systems studied.

In addition, the $\langle T_z\rangle$ term in the spin sum rule is negligible only for atoms in cubic symmetry. For atoms in noncubic environments such as surfaces and interfaces, as seen from Table 3, its importance

Table 6
Calculated values of $\langle L_z\rangle$, $\langle S_z\rangle$, $\langle T_z\rangle$, $\langle S_e\rangle$ and N_h and sum rule errors $R_1 = I_m/I_t/\langle L_z\rangle/2N_h - 1$, $R_2 = I_s/I_t/\langle S_e\rangle/N_h - 1$ and $R_3 = I_m/I_s/\langle L_z\rangle/2S_e - 1$ for Ni(0 0 1), Co(0 0 0 1) and Fe(0 0 1) surface (S) and bulk-like center (C) layers

Atom	$\langle L_z\rangle$	$\langle S_z\rangle$	$7\langle T_z\rangle$	$\langle S_e\rangle$	N_h	R_1	R_2	R_3
Ni(S)	− 0.069	− 0.67	− 0.082	− 0.250	1.81	0.27	0.52	− 0.10
Ni(C)	− 0.051	− 0.62	− 0.027	− 0.215	1.66	0.20	0.36	− 0.11
Co(S)	− 0.090	− 1.61	0.240	− 0.457	2.60	0.11	0.24	− 0.09
Co(C)	− 0.078	− 1.52	0.014	− 0.502	2.55	0.09	0.22	− 0.10
Fe(S)	− 0.111	− 2.71	0.230	− 0.828	3.70	0.10	0.16	− 0.04
Fe(C)	− 0.063	− 2.10	0.028	− 0.691	3.34	0.04	0.15	− 0.09

is obvious, since its magnitude becomes 8.5%, 12% and 15% of $\langle S_z\rangle$ for Fe(0 0 1), Ni(0 0 1) and Co(0 0 0 1), respectively. The hybridization between different l shells is the main mechanism causing the failure of the MCD spin sum rule for transition metals [111–113]. Recently, these sum rules have been extensively applied for the determination of spin and orbital magnetic moments, magnetic ordering and element-specific hysteresis and MCA energies (a more comprehensive review is given by J. Stöhr in this issue).

Based on a second-order perturbation theory, Bruno [18] showed that E_{MCA} in magnetic thin films can be related to the anisotropy of the orbital magnetic moment ($\langle L_z\rangle - \langle L_x\rangle$). This model was corroborated by Weller et al. [115] and Dürr et al. [116], who measured the value of $\langle L_z\rangle - \langle L_x\rangle$ for Au/Co/Au, Ni and Co/Ni thin films with the MCD sum rules. However, the relation is not universally valid. As pointed out very recently by van der Laan [117], the proportionality between E_{MCA} and $\langle L_z\rangle - \langle L_x\rangle$ relies on an assumption that all d-holes are in the minority spin band. This condition is usually satisfied for Co and Ni systems but not for Fe systems. As listed in Table 1, for example, E_{MCA} shows no correlation (it even differs in sign) with ΔM_L for the Fe monolayer.

5. Conclusions

In summary, state-of-the-art ab initio density functional electronic structure calculations that include SOC have achieved great success in the exciting field of thin film magnetism, in both explaining existing phenomena and, more importantly, in predicting the properties of new systems. Illustrative results demonstrate that the magnetic anisotropy and magnetostriction can be predicted correctly using the state-tracking and torque procedures; MOKE and X-ray MCD can be explained in the frame work of interband transitions. In the future, electronic structure theory is expected to continuously play a predictive role by considering more practical systems, by eliminating the limitation of the local spin density approximation and by developing more efficient and precise methods.

Acknowledgements

We thank Drs. K.B. Hathaway, D.S. Wang, L.J. Chen, L.P. Zhong, M.Y. Kim, A. Shick, X.D. Wang and V.I. Gavrilenko for stimulating discussions and collaborations. Work supported by the ONR (Grant Nos. N00014-95-1-0489 and N00014-94-1-0030), a seed grant from the Parson's foundation, and by computing grants at the ARSC and NAVO.

References

[1] A.J. Freeman, R.Q. Wu, J. Magn. Magn. Mater. 100 (1991) 497.
[2] R.Q. Wu, A.J. Freeman, Phys. Rev. B 51 (1995) 5408.
[3] S. Blügel, Phys. Rev. Lett. 68 (1992) 851.
[4] O. Eriksson, R.C. Albers, A.B. Boring, Phys. Rev. Lett. 66 (1991) 1350.
[5] A.M.N Nikllasson et al., Phys. Rev. B 56 (1997) 3276.

[6] T. Lin, M.A. Tomaz, M.M. Schwickert, G.R. Harp, Phys. Rev. B 58 (1998) 862.
[7] M.N. Baibich, J.M. Broto, A. Fert, A. Dau, F. Petroff, P. Eitenne, G. Creuzet, A. Friederich, J. Chazelas, Phys. Rev. Lett. 61 (1988) 2472.
[8] G. Binasch, P. Grunberg, F. Saurenbach, W. Zinn, Phys. Rev. B 39 (1989) 4828.
[9] S.S.P. Parkin, N. More, K.P. Roche, Phys. Rev. Lett. 64 (1990) 2304.
[10] B. Dieny, V.S. Speriosu, S.S.P. Parkin, A. B Gurney, D.R. Wilhoit, D. Mauri, Phys. Rev. B 43 (1991) 1279.
[11] E. Wimmer, H. Krakauer, M. Weinert, A.J. Freeman, Phys. Rev. B 24 (1981) 864.
[12] M. Weinert, E. Wimmer, A.J. Freeman, Phys. Rev. B 26 (1982) 4571, and references therein.
[13] L. Néel, J. Phys. Radium 15 (1954) 225.
[14] M.T. Johnson, P.J.H. Bloemen, F.J.A. den Broeder, J.J. de Vries, Rep. Prog. Phys. 59 (1996) 1409.
[15] J.H. van Vleck, Phys. Rev. 52 (1937) 1178.
[16] H. Brooks, Phys. Rev. 58 (1940) 909.
[17] G.C. Fletcher, Proc. Roy. Soc. London 67 A (1954) 505.
[18] P. Bruno, Phys. Rev. B 39 (1989) 865.
[19] P. Bruno, J.P. Renard, Appl. Phys. A 49 (1989) 499.
[20] J.G. Gay, R. Richter, Phys. Rev. Lett. 56 (1986) 2728.
[21] J.G. Gay, R. Richter, J. Appl. Phys. 61 (1987) 3362.
[22] G.H.O. Daalderop, P.J. Kelly, M.F.H. Schuurmans, Phys. Rev. B 42 (1990) 1533.
[23] A.R. Mackintosh, O.K. Andersen, in: M. Springford (Ed.), Electrons at the Fermi Surface, Cambridge University Press, Cambridge, 1980.
[24] X.D. Wang, D.S. Wang, R.Q. Wu, A.J. Freeman, J. Magn. Magn. Mater. 159 (1996) 337.
[25] D.S. Wang, R.Q. Wu, A.J. Freeman, Phys. Rev. Lett. 70 (1993) 869.
[26] D.S. Wang, R.Q. Wu, A.J. Freeman, Phys. Rev. Lett. 71 (1993) 2166.
[27] X.D. Wang, R.Q. Wu, D.S. Wang, A.J. Freeman, Phys. Rev. B 54 (1996) 61.
[28] D.S. Wang, R.Q. Wu, A.J. Freeman, Phys. Rev. B 47 (1993) 14932.
[29] D.S. Wang, R.Q. Wu, A.J. Freeman, J. Magn. Magn. Mater. 129 (1994) 327.
[30] A. Lessard, T.H. Moos, W. Hübner, Phys. Rev. B 56 (1997) 2594, and references therein.
[31] J.P. Perdew et al., Phys. Rev. B 33 (1986) 8800.
[32] J.P. Perdew et al., Phys. Rev. B 46 (1992) 6671.
[33] U. von Barth, L. Hedin, J. Phys. C 5 (1972) 1629.
[34] P.A. Gacia, A.D. Meinholdt, A. Suna, Appl. Phys. Lett. 47 (1985) 178.
[35] P. Krams, F. Lauks, R.L. Stamps, B. Hillebrands, G. Güntherodt, Phys. Rev. Lett. 69 (1992) 3674.
[36] B.N. Engel, M.H. Wiedmann, C.M. Falco, J. Appl. Phys. 75 (1994) 6401.
[37] F. Huang, G.J. Mankey, R.J. Willis, J. Appl. Phys. 75 (1994) 6406.
[38] W. Weber et al., Phys. Rev. B 54 (1996) 4075.
[39] S. Hope, E. Gu, B. Choi, J.A. Bland, Phys, Rev. Lett. 80 (1998) 1750.
[40] J.E. Hurst Jr., W.J. Kozlovsky, Jpn. J. Appl. Phys. 32 (1993) 5301.
[41] R.Q. Wu, V.I. Gavrilenko, Phys. Rev. B, in press.
[42] R.Q. Wu, A.J. Freman, J. Appl. Phys. 79 (1996) 6500.
[43] R.Q. Wu, L.J. Chen, A.J. Freeman, J. Magn. Magn. Mater. 170 (1997) 103.
[44] A.B. Shick, D.L. Novikov, A.J. Freeman, Phys. Rev. B 56 (1997) R14259.
[45] A.B. Shick, D.L. Novikov, A.J. Freeman, J. Appl. Phys. 83 (1998) 7258.
[46] D.S. Wang, R.Q. Wu, A.J. Freeman, J. Magn. Magn. Mater. 129 (1994) 327.
[47] L. Szunyogh, B. Ujfalussy, U. Pustogowa, P. Weinberger, Phys. Rev. B 57 (1998) 8838.
[48] L. Zhong, M. Kim, X. Wang, A.J. Freeman, Phys. Rev. B 53 (1996) 9770.
[49] M. Kim, L. Zhong, A.J. Freeman, Phys. Rev. B 57 (1998) 5271.
[50] W. Weber et al., Nature 374 (1995) 788.
[51] W. Weber et al., Phys. Rev. Lett. 76 (1996) 1940.
[52] L.P. Zhong, X.D Wang, A.J. Freeman, IEEE Trans. Magn. bf 34 (1998) 1213.
[53] A.B. Shick, Yu.N. Gornostyrev, A.J. Freeman, J. Appl. Phys., in press.
[54] R.K. Kawakami et al., Phys. Rev. Lett. 77 (1996) 2570.
[55] R.K. Kawakami et al., Phys. Rev. B 58 (1998) R5924.
[56] H.J. Choi et al., Phys. Rev. B 57 (1998) R12713.
[57] G.H.O. Daalderop, P.J. Kelly, M.F.H. Schuurmans, Phys. Rev. B 41 (1990) 11919.
[58] G.Y. Guo, W.M. Temmerman, H. Ebert, Physica B 172 (1991) 61.
[59] P. Strange, J.B. Sraunton, B.L. Gyorffy, H. Ebert, 172 (1991) 51.
[60] J. Trygg, B. Johnansson, O. Eriksson, J.M. Wills, Phys. Rev. Lett. 75 (1995) 2871.
[61] S.V. Halilov, A. Ya. Perlov, P.M. Oppeneer, A.N. Yaresko, V.N. Antonov, Phys. Rev. B 57 (1998) 9557.
[62] S.V. Beiden et al., Phys. Rev. B 57 (1998) 14247.
[63] O. Eriksson et al., Phys. Rev. B 41 (1990) 7311.
[64] O. Eriksson et al., Phys. Rev. B 42 (1990) 2707.
[65] J.R. Cullen, A.E. Clark, K.B. Hathaway, in: R.W. Cahn, P. Hasen, E.J. Kramer (Eds.), Materials Science and Technology, vol. IIIB, 1994, p. 529.
[66] B. Schulz, K. Baberschke, Phys. Rev. B 50 (1994) 13467.
[67] L.J. Chen, R.Q. Wu, A.J. Freeman, J. Appl. Phys. 81 (1997) 4417.
[68] M. Farle, W. Platow, A.N. Anisimov, P. Poulopoulos, K. Baberschke, Phys. Rev. B 55 (1997) 3708.
[69] M. Farle, W. Platow, A.N. Anisimov, P. Poulopoulos, K. Baberschke, Phys. Rev. B 56 (1997) 5100.
[70] O. Hjorstam, K. Baberschke, J.M. Wills, B. Johansson, O. Eriksson, Phys. Rev. B 55 (1997) 15026.

[71] D. Bonnenberg, K.A. Hempel, H.P.J. Wijn, in: H.P.J. Wijn, Landolt-Bornstein (Eds.), Numerical Data and Functional Relationships in Science and Technology, New Series, Group 3, vol. 19a Springer, Berlin, 1986.
[72] E.W. Lee, M.A. Asgar, Proc. Roy. Soc. London Ser. A 326 (1971) 73.
[73] D.I. Bower, Proc. Roy. Soc. London Ser. A 326 (1971) 87.
[74] S. Chikazumi, Physics of Magnetism, Krieger, Malabar, FL, 1986.
[75] H.P.J. Wijn (Ed.), Data in Science and Technology: Magnetic Properties of Metals, Springer, Berlin, 1986.
[76] R.Q. Wu, L.J. Chen, A. Shick, A.J. Freeman, J. Magn. Magn. Mater. 177–181 (1998) 1216.
[77] A.E. Clark, in: E.P. Wohlfarth (Ed.), Ferromagnetic Materials vol. 1, North-Holland, Amsterdam, p. 531.
[78] K.N.R. Taylor, Adv. Phys. 2 (1971) 551.
[79] K. Hathaway, J. Cullen, J. Phys. Condens. Matter 3 (1991) 8911.
[80] R.Q. Wu, J. Appl. Phys. 85 (1999) 6217.
[81] S.D. Bader, J. Magn. Magn. Mater. 100 (1991) 440, and references therein.
[82] R. Kubo, J. Phys. Soc. Jpn. 12 (1957) 570.
[83] C.S. Wang, J. Callaway, Phys. Rev. B 9 (1974) 4897.
[84] H. Ebert, Rep. Prog. Phys. 59 (1996) 1665.
[85] P.M. Oppeneer, T. Maurer, J. Sticht, J. Kübler, Phys. Rev. B 45 (1992) 10924.
[86] G.Y. Guo, H. Ebert, Phys. Rev. B 50 (1994) R10377.
[87] G.Y. Guo, H. Ebert, Phys. Rev. B 51 (1995) 12633.
[88] N. Mainkar, D.A. Browne, J. Callaway, Phys. Rev. B 53 (1996) 3692.
[89] T. Casche, M.S.S. Brooks, B. Johansson, Phys. Rev. B 53 (1996) 296.
[90] A.J. Freeman, R.Q. Wu, L.J. Chen, L.P. Zhong, MRS Proc. (1999), in press.
[91] Y.A. Uspenskii, E.T. Kulatov, S.V. Kaalilov, Phys. Rev. B 54 (1996) 474.
[92] S.P. Lim, D.L. Price, B.R. Cooper, IEEE Trans. Magn. 27 (1991) 3648.
[93] P.M. Oppeneer, M.S.S. Brooks, V.N. Antonov, T. Kraft, H. Eschrig, Phys. Rev. B 53 (1996) R10437.
[94] P.M. Oppeneer, V.N. Antonov, in: H. Ebert, G. Schütz (Eds.), Spin–Orbit Influenced Spectroscopies of Magnetic Solid, Springer, Berlin, 1996, p. 29.
[95] A.I. Lichtenstein, V.P. Antropov, B.N. Harmon, Phys. Rev. B 49 (1995) R10770.
[96] A.N. Yaresko et al., Europhys. Lett. 36 (1996) 551.
[97] M.Y. Kim, R.Q. Wu, A.J. Freeman, Phys. Rev. 59 (1999) 9432.
[98] V.I. Gavrilenko, R.Q. Wu, J. Appl. Phys. 85 (1999).
[99] K. Sato, J. Abe, H. Ikekame, K. Takanashi, S. Mitani, H. Fujimori, J. Magn. Soc. Jpn. Suppl. 20 (1996) S1.
[100] K. Takanashi, S. Mitani, H. Fujimori, K. Sato, Y. Suzuki, J. Magn. Magn. Mater. 177–181 (1998) 1199.
[101] D. Weller et al., Phys. Rev. Lett. 72 (1994) 2097.
[102] G.R. Harp et al., Phys. Rev. B 48 (1993) 17538.
[103] G.Y. Guo, H. Ebert, Phys. Rev. B 50 (1994) 10377.
[104] P.M. Oppeneer, T. Kraft, H. Eschrig, Phys. Rev. B 52 (1995) 3577.
[105] J.M. MacLaren, W. Huang, J. Appl. Phys. 79 (1996) 6196.
[106] R.Q. Wu, unpublished.
[107] G. Schütz, W. Wagner, W. Wilhelm, P. Kienle, R. Zeller, G. Materlik, Phys. Rev. Lett. 58 (1987) 737.
[108] J. Stöhr, Science 259 (1993) 658.
[109] B. T Thole, P. Carra, F. Sette, G. van der Laan, Phys. Rev. Lett. 68 (1992) 1943.
[110] P. Carra, B.T. Thole, M. Altarelli, X-D. Wang, Phys. Rev. Lett. 70 (1993) 694.
[111] R.Q. Wu, D.S. Wang, A.J. Freeman, Phys. Rev. Lett. 71 (1993) 3581.
[112] R.Q. Wu, D.S. Wang, A.J. Freeman, Phys. Rev. Lett. 73 (1994) 1994.
[113] R.Q. Wu, D.S. Wang, A.J. Freeman, J. Magn. Magn. Mater. 132 (1994) 103.
[114] C.T. Chen et al., Phys. Rev. Lett. 75 (1995) 152.
[115] D. Weller et al., Phys. Rev. Lett 75 (1995) 3752.
[116] H.A. Dürr et al., Science 277 (1997) 213.
[117] G. van der Laan, Phys. Rev. Lett. 82 (1999) 640.
[118] D.S. Wang, R.Q. Wu, A.J. Freeman, Phys. Rev. B 48 (1993) 15883.
[119] B. Ujfalussy, L. Szunyogh, P. Weinberger, Phys. Rev. B 54 (1996) 9883.
[120] G.Y. Guo, W.M. Temmerman, H. Ebert, J. Phys. C 3 (1991) 8205.
[121] G.Y. Guo, W.M. Temmerman, H. Ebert, J. Magn. Magn. Mater. 104–107 (1992) 1772.
[122] C. Li, A.J. Freeman, H.J.F. Jansen, C.L. Fu, Phys. Rev. B 42 (1990) 5433.
[123] L. Szunyogh, B. Ujfalussy, P. Weinberger, Phys. Rev. B 51 (1995) 9552.